The ORF3 Protein of Hepatitis E Virus Interacts with Hemopexin by Means of Its 26 Amino Acid N-Terminal Hydrophobic Domain II†

Ruchi Ratra, Anindita Kar-Roy, and Sunil K. Lal*

Virology Group, International Centre for Genetic Engineering and Biotechnology, P.O. Box 10504, Aruna Asaf Ali Marg, New Delhi-110067, India

Received August 16, 2007; Revised Manuscript Received December 10, 2007

ABSTRACT: Hepatitis E virus (HEV) is a nonenveloped plus-stranded RNA virus that is a major cause of acute hepatitis in many developing countries. Recent work has shown HEV may be endemic in developed countries also. The 5′ two-thirds of the 7.2 kb single-stranded RNA genome of HEV encodes ORF1, and the 3′ end encodes the structural proteins ORF2 and ORF3. ORF1 is the nonstructural protein involved in viral RNA synthesis, and ORF2 is the major capsid protein, whereas ORF3 is a very small protein of only 123 amino acids. The precise cellular functions of ORF3 protein remain obscure, although it has been postulated to be a viral regulatory protein. To elucidate the role of ORF3 in viral pathogenesis, the yeast two-hybrid system was used to screen a human liver cDNA library for proteins interacting with ORF3. One of the ORF3-interacting partners thus isolated and identified was hemopexin, a 60 kDa acute-phase plasma glycoprotein with a high binding affinity to heme. The two-hybrid result was validated by *in vitro* pull-down and co-immunoprecipitation assays and finally by intracellular fluorescence resonance energy transfer. Using a deletion mapping approach, the hydrophobic domain II of ORF3 (spanning amino acids 37 to 62) was found to be responsible for binding to Hpx, with amino acids 63 to 77 possibly contributing to the strength of the interaction. The biological significance of this interaction in the virus life cycle has been discussed.

Hepatitis E virus (HEV[1]) infection results in hepatitis E, an acute and self-limiting disease. The disease is prevalent in much of the developing world where HEV is known to cause large epidemics (*1*−*3*). Recent work has shown that HEV may be more common in developed countries than originally thought (*4*−*6*). HEV is transmitted primarily by the fecal−oral route, and fecally contaminated drinking water is the most commonly documented vehicle of transmission. However, recently it has been shown that eating raw or undercooked meat might directly transmit HEV, suggesting that hepatitis E may be a zoonotic disease (*7*).

The studies on HEV molecular biology and pathogenesis have been severely restricted by the lack of an efficient cell culture system for the virus and small animal models of viral infection. In order to study different aspects of the virus, the individual viral proteins are routinely expressed subgenomically from plasmid vectors. The 7.2 kb positive-sense single-stranded RNA genome of HEV codes for three proteins: ORF1, ORF2 and ORF3 (*3*). ORF1 is the putative nonstructural polyprotein proposed to be involved in viral RNA synthesis (*8*). ORF2 is the major capsid protein and has been shown to be a viral glycoprotein, expressed both intracellularly and on the cell surface (*9*), and also to bind to the 5′ region of viral RNA (*10*). ORF3 is a small 123 amino acid protein currently of unknown function. It is a viral phosphoprotein that associates with the cytoskeleton upon cell fractionation (*11*), interacts with the ORF2 protein (*12*), binds to src homology 3 domains of cellular signal transduction proteins (*13*) and interacts with the liver specific α_1-microglobulin bikunin precursor (*14*) and its two processed proteins, α_1-microglobulin (*14*) and bikunin (*15*). Recently our lab has also shown that enhanced α_1-microglobulin secretion from ORF3 expressing human hepatoma cells is mediated by the tumor susceptibility gene 101 (*16*). All this clearly suggests that the ORF3 protein may have multifarious regulatory functions.

In an effort to elucidate the properties of the ORF3 protein, we opted for an approach to screen for host proteins that interact with it. The yeast two-hybrid system has been well documented as a good tool for screening and isolating interacting partners (*17*). Using the ORF3 protein as "bait", we screened a human liver cDNA library and identified human hemopexin (Hpx) as an interacting partner. Hpx is a liver specific 60 kDa heme-binding acute-phase plasma glycoprotein that transports heme to the liver for breakdown and iron recovery (*18*). The ORF3−Hpx interaction was validated using coupled transcription−translation pull-down assays and co-immunoprecipitation experiments. When co-expressed in COS-1 cells, ORF3 and Hpx colocalized, and using variant enhanced green fluorescent protein (EGFP)

† This work was supported by internal funds from the International Centre for Genetic Engineering & Biotechnology, New Delhi.

* Corresponding author. E-mail address: sunillal@icgeb.res.in. Tel: 91-11-26177357. Fax: 91-11-26162316.

[1] Abbreviations: HEV, hepatitis E virus; ORF, open reading frame; Hpx, hemopexin; FRET, fluorescence resonance energy transfer; AD, activation domain; BD, binding domain; cys/met, cysteine/methionine; Ni-NTA, nickel nitrilotriacetic acid; SDS−PAGE, sodium dodecyl sulfate-polyacrylamide gel electrophoresis; PBS, phosphate buffered saline; IP, immunoprecipitation; MFI, mean fluorescence intensity; 3-AT, 3-amino-1, 2, 4-triazole; MMPs, matrix metalloproteinases.

10.1021/bi7016552 CCC: $40.75
Published on Web 01/23/2008

fusions the interaction was further confirmed by fluorescence resonance energy transfer (FRET) imaging microscopy. Deletion analysis identified the 26 amino acid N-terminal hydrophobic domain II of the ORF3 protein as the region responsible for interacting with Hpx. Our data also suggests that the 15 amino acid region downstream to the interaction domain may contribute toward strength of this interaction. The biological significance of this interaction and its possible role in HEV-infected hepatocytes are discussed.

EXPERIMENTAL PROCEDURES

Strains and Plasmid Constructs. A GAL4 activation domain (AD) fusion liver cDNA library in pACT2 vector (pACT2-LL) was obtained from Clontech. pAS2-ORF3 [the GAL4 binding domain (BD) fusion of ORF3], pAS2-ORF3 (S80A), pAS2-ORF3Mex, pSGI-ORF2, pSGI-ORF3 and pRSET-ORF3 have been described previously (*12*, *19*, *20*). pACT2-ORF3 (AD-ORF3) was cloned by ligating a *Sma*I/*Xho*I fragment from pSGI-ORF3 into the same sites of pACT2 vector. pAS2-Hpx (BD-Hpx) was cloned by ligating *Sma*I/*Xho*I fragment from pACT2-Hpx (AD-Hpx, library clone) into *Sma*I/*Sal*I sites in pAS2. Hpx was cloned in pSGI vector as an *Eco*RI/*Xho*I fragment from pACT2-Hpx, such that Hpx expression was under the control of T7 promoter. ORF3 and Hpx deletions for yeast two-hybrid analysis were made by designing appropriate PCR primers (Table 1) and PCR amplifying and subcloning the deletions as BD- or AD-fusions in pAS2 or pACT2 vector, respectively. Domain I (lacking amino acids 16−32) and domain II (lacking amino acids 37−62) deletions of ORF3 were made by carrying out site directed mutagenesis by the Kunkel method using single stranded pSGI-ORF3 plasmid DNA as template. The oligos used for site directed deletions are given in Table 1. Deletion mutants of Hpx were cloned in pSGI [pSGI-Hpx (251−462), pSGI-Hpx (1−250), pSGI-Hpx (181−462) and pSGI-Hpx (1−314)] as an *Eco*RI/*Xho*I fragment from the respective pACT2-Hpx mutants shown in Table 1. All mutant constructs were checked by sequencing. ORF3 (33−123), (1−77) and (1−91) used for mammalian transfections have been described before (*11*). EYFPN1-Hpx was cloned by PCR amplification of pACT2-Hpx template with forward 5′ ccgctcgagatggctagggtactgggagc 3′ and reverse 5′ tcccccgggagtgagtgcagcccaggag 3′ primers and cloning the amplified fragment at the *Xho*I/*Sma*I (underlined in the forward and reverse primers, respectively) sites of EYFPN1 (Clontech). All DNA manipulations were carried out as described by Sambrook et al. (*21*). ECFPN1-ORF3 has been described before (*22*). Yeast strains used were AH109 (MATa, trp1−901, leu2−3, 112, ura3−52, his3−200, gal4Δ, gal80Δ, LYS2::$GAL1_{UAS}$-$GAL1_{TATA}$-HIS3, $GAL2_{UAS}$-$GAL2_{TATA}$-ADE2 URA3::$MEL1_{UAS}$ $MEL1_{TATA}$-lacZ) and Y187 (MATα, ura3−52, his3−200, ade2−101, trp1−901, leu2−3, 112, gal4Δ, gal80Δ, met$^-$, URA3::$GAL1_{UAS}GAL1_{TATA}$-lacZ MEL1).

Yeast Two-Hybrid Techniques. All two-hybrid media and protocols for library screening, transformations, yeast mating, yeast plasmid isolation and filter lift and liquid β-galactosidase assays were as described in the Clontech manual for the Matchmaker GAL4 two-hybrid system and in the Clontech Yeast Protocols Handbook (available at http://www.clontech.com).

Table 1: Primers and Oligos Used To Generate ORF3 and Hpx Deletion Constructs Used in This Study[a]

ORF3/Hpx constructs	PCR primers/oligos used
pAS2-ORF3 (1−91)	FP 5′ ggaattccatatggataacatgtcttttgctgc 3′
	RP 5′ aactgcaggttggcgaacacgaggtcc 3′
pAS2-ORF3 (1−77)	FP 5′ ggaattccatatggataacatgtcttttgctgc 3′
	RP 5′ aactgcagtcggggcgaaggggttgg 3′
pAS2-ORF3 (1−63)	FP 5′ ggaattccatatggataacatgtcttttgctgc 3′
	RP 5′ aactgcaggctgagaatcaacccggtc3′
pAS2-ORF3 (83−123)	FP 5′ ggaattccatatgccggggctggacctcgt 3′
	RP 5′ aactgcagggttagcggcgcggccc 3′
pAS2-ORF3 (33−123)	FP 5′ ggaattccatatgcgccaccgcccggtcag 3′
	RP 5′ aactgcagggttagcggcgcggccc 3′
pAS2-ORF3 (63−123)	FP 5′ ggaattccatatgagcccttcgccccctatatt 3′
	RP 5′ aactgcagggttagcggcgcggccc 3′
pACT2-Hpx (251−462)	FP 5′ ggaattccatatgcctggcagaggccatggac 3′
	RP 5′ ccgctcgagtcagtgagtgcagcccagg 3′
pACT2-Hpx (1−250)	FP 5′ ggaattccatatggctagggtactgggagc 3′
	RP 5′ ccgctcgagttagcagggcatgaagtagtctcg 3′
pACT2-Hpx (56−462)	FP 5′ ggaattccatatggatgctaccaccctggatgac 3′
	RP 5′ ccgctcgagtcagtgagtgcagcccagg 3′
pACT2-Hpx (96−462)	FP 5′ ggaattccatatgcctgtggatgctgcattccg 3′
	RP 5′ ccgctcgagtcagtgagtgcagcccagg 3′
pACT2-Hpx (181−462)	FP 5′ ggaattccatatgtcctggccagctgttggga 3′
	RP 5′ ccgctcgagtcagtgagtgcagcccagg 3′
pACT2-Hpx (1−314)	FP 5′ ggaattccatatggctagggtactgggagc 3′
	RP 5′ ccgctcgagttaccaggaaaaggcagcatccac 3′
pSGI-ORF3 DI del	5′ ggttctagaccatgctctcgcgccac 3′
pSGI-ORF3 DII del	5′ ccaccgcccgagcccttcgc 3′

[a] The forward (FP) and reverse primers (RP) used to amplify the different fragments are indicated. ORF3 deletions were PCR amplified using pSGI-ORF3 as template and cloned in pAS2 vector using *Nde*I and *Pst*I sites (underlined) in FP and RP, respectively, to generate ORF3 truncated proteins as a fusion to the BD. Hpx deletions were PCR amplified using pACT2-Hpx as template and cloned in pACT2 vector using *Eco*RI and *Xho*I sites (underlined) in FP and RP respectively, to generate Hpx truncated proteins as a fusion to the AD. The numbers in parentheses represent the first and the last amino acids of the region included in the protein. pSGI-ORF3 DI and DII del represent ORF3 protein in which domain I (spanning amino acids 16−32) and domain II (spanning amino acids 37−62) were deleted, respectively.

In Vitro Transcription−Translation Assay. pSGI-Hpx and its truncations or pSGI-ORF3 construct was employed in a coupled *in vitro* transcription−translation carried out with the TNT T7 quick coupled reticulocyte lysate system (Promega) according to the manufacturer's guidelines in the presence of [^{35}S] cysteine/methionine (cys/met) promix (New England Nuclear) to radiolabel the synthesized proteins.

In Vitro Histidine Pull-Down Assay. The prokaryotic expression vector, pRSET-ORF3, for ORF3 expression and production of the recombinant N-terminal hexa histidine tagged ORF3 (His_6-ORF3) protein in *Escherichia coli* BL21 (DE3) cells has been reported previously (*20*). Briefly, after induction, the *E. coli* cells were pelleted and resuspended in binding buffer (Tris-phosphate buffer, pH 8.0 containing 1 mM PMSF and 20 mM β-ME). The bacterial pellet was digested with lysozyme and subjected to three cycles of freeze−thawing in liquid nitrogen. The His_6-ORF3 protein was obtained in the pellet fraction of the post-freeze−thawed sample as insoluble inclusion bodies. The inclusion bodies were then solubilized in the binding buffer containing 8 M urea, and His_6-ORF3 protein was purified by nickel-chelate affinity chromatography on precharged Ni-NTA beads (Qiagen) according to the manufacturer's instructions. These ORF3 bound beads were used directly for histidine pull-down assays. Only Ni-NTA beads served as control. The beads were washed three times in binding buffer. To the

washed beads resuspended in 500 μL of binding buffer was added 5 μL of [^{35}S] labeled *in vitro* translated Hpx protein. Beads were incubated for 1 h at 4 °C with constant shaking. The beads were again washed, and bound protein complexes were analyzed by adding 20 μL of 2X SDS sample buffer, boiling for 10 min and then resolving by 8% SDS−PAGE. Bands were detected by fluorography.

Cell Culture and Transfection. HuH-7 and COS-1 cells were maintained at 37 °C and 5% CO_2 in Dulbecco's modified Eagle's medium (DMEM, Gibco) supplemented with 10% fetal bovine serum, 100 U/mL penicillin and 0.1 mg/mL streptomycin. Cells were transfected at 60% confluency with Lipofectamine Plus reagent (Life Technologies) according to the manufacturer's instructions. Cells were transfected in either a 60 or 100 mm culture dish (for immunoprecipitation) or a 6-well culture plate on glass cover slips (for immunofluorescence microscopy).

Metabolic Labeling and Immunoprecipitation. At 44 h post-transfection cells were washed twice with 1X PBS and starved for 1 h in cys/met deficient medium and were then labeled with 100 μCi/mL of [^{35}S] cys/met promix for 4 h. After 4 h the cells were washed once with 1X PBS and lysed in 500 μL of immunoprecipitation (IP) buffer (20 mM Tris-Cl, pH 7.5; 150 mM NaCl; 1% Triton X-100; 1 mM EDTA; 1 mM EGTA; 2.5 mM sodium pyrophosphate; 1 mM β-glycerol phosphate; 1 mM sodium orthovanadate) supplemented with protease inhibitor cocktail. The lysates were collected and clarified by centrifugation for 10 min at 13,000 rpm. For immunoprecipitation, an equal amount of protein determined by protein quantification assay (Bio-Rad) was incubated with 1 μg of corresponding antibody overnight at 4 °C, followed by incubation with 100 μL of 10% protein A Sepharose suspension for 1 h. Beads were washed three times in the IP buffer, boiled in 2X SDS sample buffer and resolved by SDS−PAGE followed by immunoblotting or fluorography.

Immunoblotting. The immunoprecipitated proteins were resolved by SDS−PAGE and electroblotted onto nitrocellulose membranes. The membranes were blocked with 5% BSA for 1 h and then incubated with respective primary antibody, again washed and incubated with appropriate HRP conjugated secondary antibody. The proteins were then detected by the ECL (enhanced chemiluminescence) detection method (Cell Signaling Technology) according to the manufacturer's protocol.

Microscopy and FRET Analysis. The procedure for colocalization and FRET analysis has been described previously (*22*). COS-1 cells plated on coverslips were transfected with ECFP-ORF3 and EYFP-Hpx expression constructs. FRET was detected using the acceptor photobleaching approach as described before (*22*). The increase in ECFP emission, which is a direct measure of FRET efficiency, denoted as *E*%, was calculated as [1 − (ECFP emission before EYFP photobleach/ECFP emission after EYFP photobleach) × 100]. Superimposition of images was done using Adobe Photoshop 6.0 software.

RESULTS

The ORF3 Protein of HEV Interacts with Hemopexin. To identify host proteins that interact with the ORF3 protein of HEV, the matchmaker GAL4 based yeast two-hybrid system (Clontech) was used to screen a human liver cDNA library. Library scale screening was performed on 2×10^6 cotransformants. AH109 was transformed with pAS2-ORF3 and then sequentially transformed with the liver cDNA library (pACT2-LL). The cotransformants that contain positive interacting partners with the bait protein result in the activation of transcription of the three reporter genes: histidine, adenine and β-galactosidase lac Z gene. Thus the cotransformants obtained above were tested for histidine (His^+) and adenine (Ade^+) prototrophy by first plating on triple negative synthetic dropout media SD-$leu^-trp^-his^-$, and grown colonies were further selected on quadruple negative media SD-$leu^-trp^-his^-ade^-$and subsequently confirmed positive on the filter β-galactosidase assay. The cDNA inserts from the $His^+Ade^+\beta$-gal^+ clones were sequenced to identify the interacting partner. Sequence comparisons were done by FASTA searches of the GenBank database (http://www.ncbi.nlm.nih.gov/). One such clone identified from the screening was human hemopexin (Hpx) mRNA, GenBank reference sequence NM_000613. The ~1.6 kb full-length cDNA was independently isolated from 5 different clones from the library screen.

Yeast Two-Hybrid Analysis of ORF3−Hpx Interaction. In order to confirm the ORF3−Hpx interaction, the AD-Hpx/library clone was reintroduced into AH109 along with BD-ORF3 (Figure 1A). Self-association of ORF3, that has been reported earlier (*23*), was used as a positive control for the yeast two-hybrid assay. The empty BD- and AD- vectors and bait (BD-ORF3) and prey (AD-Hpx) alone or in combination (BD- + AD- and BD- + AD-Hpx) served as negative controls. Our results show that the histidine, adenine and β-galactosidase reporter activity was specifically turned on only when ORF3 and Hpx were present together inside the yeast host, allowing growth on SD-$leu^-trp^-his^-ade^-$ and blue color by the filter β-galactosidase assay. A quantitative estimation of the relative strengths of interaction between ORF3 and Hpx in comparison to controls as judged by liquid β-galactosidase assay is also shown graphically in Figure 1A. The liquid β-galactosidase levels of ORF3−Hpx cotransformant was almost 30 fold higher compared to the negative controls and about 1.3 fold of the positive control. The histidine reporter construct has residual histidine expression that is overcome by growing cells in the presence of 3-amino-1,2,4-triazole (3-AT). Only the ORF3 and Hpx cotransformants and the positive controls were able to grow in the presence of 50 mM 3-AT, clearly displaying specificity and strength of the interaction.

To eliminate false positives, a common problem with interactions obtained from a library screen, and to assay the specificity of a two-hybrid interaction, it is necessary to reconfirm the two-hybrid interaction by a series of additional transformations. The ORF3−Hpx interaction was thus verified using the yeast mating protocol, a convenient method of introducing two plasmids into the same host cells. The AH109 strain (mating type a) was transformed with BD-ORF3 and Y187 (mating type α) with AD-Hpx. The two strains were mated, and diploids were analyzed for reporter gene activity. All appropriate positive and negative controls were used as above. The results (Figure 1B) again showed that diploid cells are able to grow on SD-$leu^-trp^-his^-ade^-$ only when they harbor both ORF3 and Hpx constructs. Additionally when Hpx was switched from AD- to the DNA-

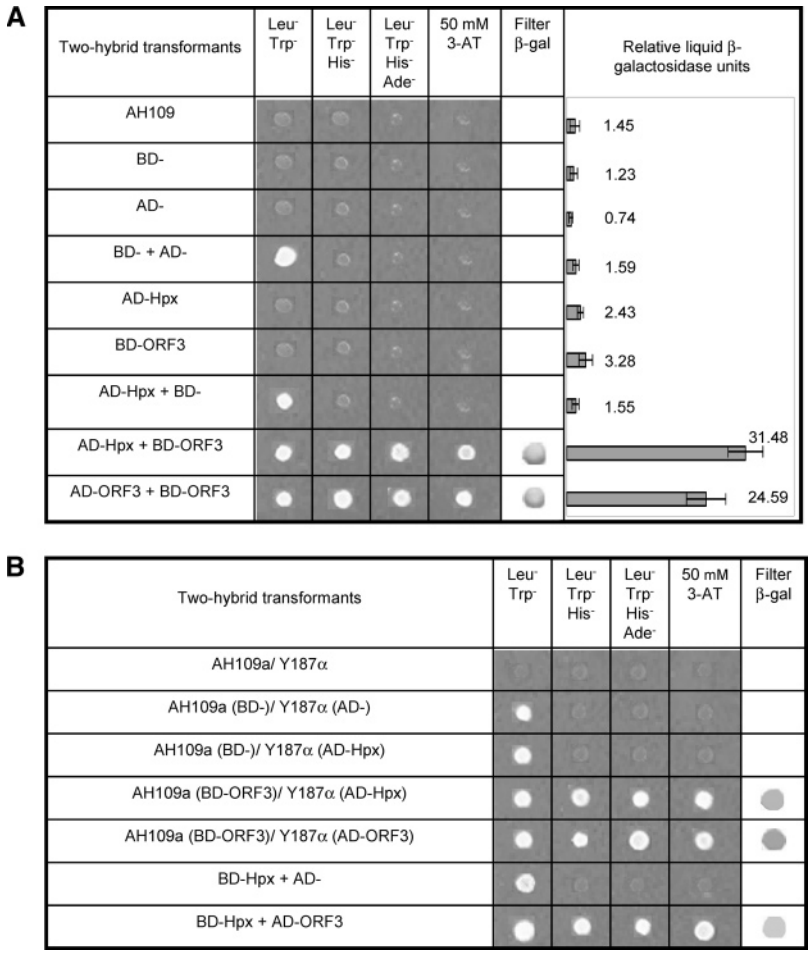

FIGURE 1: Yeast two-hybrid analysis of ORF3−Hpx interaction. (A) Yeast strain AH109 was singly transformed or co-transformed with empty BD- and AD- vectors or fused BD- and AD- expression constructs of ORF3 and Hpx. AH109 is the untransformed yeast host strain. AD-ORF3 + BD-ORF3 co-transformant is the positive control for the yeast two-hybrid assay. AD-Hpx + BD- is the negative control indicating reporter gene activity is specifically turned on only in presence of ORF3. Yeast cells were plated on synthetic dropout medium lacking leucine and tryptophan (leu^-trp^-) as co-transformation controls and to medium lacking histidine (his^-) and adenine (ade^-) to select for yeast two-hybrid interactions at moderate ($leu^-trp^-his^-$) and high ($leu^-trp^-his^-ade^-$) stringency. 50 mM AT represents $leu^-trp^-his^-ade^-$ medium to which 50 mM 3-amino-1, 2, 4-triazole has been added. Yeast plates were incubated at 30 °C for 4 days. β-gal represents the filter lift β-galactosidase assay. The horizontal bar graph represents relative β-galactosidase units determined from the liquid β-gal assay. (B) Results of yeast two-hybrid retest with Hpx. AH109a (mating type a) and Y187α (mating type α) are two haploid host cells transformed with either BD- or AD- plasmids or fused BD- and AD- expression constructs of ORF3 and Hpx. The diploid cells (separated by a slash, /), harboring both the ORF3 and Hpx expression constructs turn on the reporter gene activity. The abbreviations used and negative and positive controls are as described above. A positive two-hybrid interaction was also obtained when the Hpx- protein was expressed as a fusion to the BD- vector instead of to AD- and ORF3 vice versa (domain swapping).

BD vector and ORF3 from the BD- to the AD- vector (domain swapping), a positive two-hybrid interaction was again obtained, indicating that ORF3−Hpx interaction is independent of the fused domains.

In Vitro Verification of ORF3−Hpx Interaction. Once Hpx that interacts with ORF3 was isolated from the library screen, the next immediate challenge was to confirm this interaction outside the yeast two-hybrid system. We thus performed *in vitro* histidine pull-down and co-immunoprecipitation assays. First, *E. coli* BL21 (DE3) cells were transformed with pRSET-ORF3 and processed as described under Experimental Procedures. The His_6-ORF3 protein expression and the protein bound to the Ni-NTA beads was verified by Coomassie blue staining and by Western blot with anti-his antibody (data not shown). Expression of Hpx from pSGI-Hpx expression construct was also verified using *in vitro* coupled transcription−translation to produce [^{35}S] labeled protein of ~52 kDa as detected by fluorography (Figure 2A, lane 3). The labeled Hpx protein was then incubated either with the Ni-NTA beads alone or with beads to which His_6-ORF3 was bound. The Hpx protein was recovered by the Ni-NTA-His_6-ORF3 fusion protein (lane 1) but not by Ni-NTA alone (lane 2). The results indicate that Hpx interacts specifically with the ORF3 portion of the Ni-NTA-His_6-ORF3 fusion protein. Although Hpx protein bound to Ni-NTA-His_6-ORF3 (lane 1) represented 50% of the total input (lane 3), the binding was reproducible in multiple experiments. This low percentage of binding could be due to imperfect binding conditions, an absence of necessary cofactors, or the failure of translated Hpx to achieve an authentic native conformation or modification.

Similar mixing experiments were performed with COS-1 cell extracts in place of *in vitro* translated Hpx. Hpx was cloned with a C-terminal EYFP tag in mammalian expression vector, pEYFPN1. COS-1 cells were transfected with the pEYFPN1-Hpx construct. The cells were metabolically labeled and the cell lysate was immunoprecipitated with anti-GFP antibody or preimmune sera. After washing three times

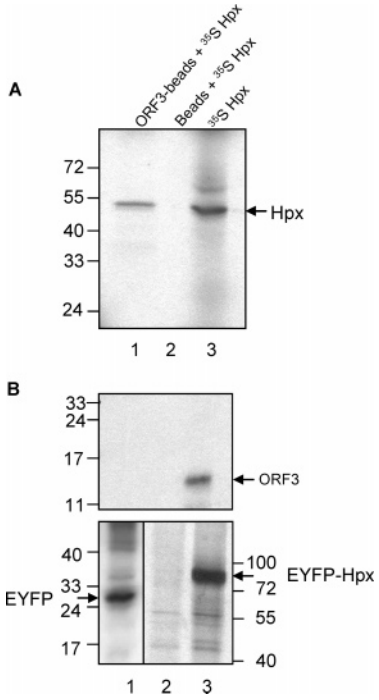

FIGURE 2: *In vitro* verification of ORF3 interaction with Hpx. (A) His_6-ORF3 protein was expressed in *E. coli* and bound to Ni-NTA beads. Equal amount of *in vitro* expressed radiolabeled [^{35}S] Hpx was added to His_6-ORF3 bound to Ni-NTA beads (lane 1) or to Ni-NTA beads alone (lane 2). Lane 3 is the amount of [^{35}S] Hpx used for each reaction. Samples were resolved by 8% SDS−PAGE and bands detected by fluorography. The numbers to the left-hand side of the panel indicate the position and size of the molecular weight markers in kDa. (B) COS-1 cells were transfected with EYFPN1-Hpx expression construct (lanes 2 and 3) and immunoprecipitated with anti-GFP antibody (lower panel, lane 3) or with preimmune sera (lane 2). Samples were resolved by 8% SDS−PAGE and band detected by fluorography. Lower panel, lane 1 shows EYFPN1 transfected cells from which EYFP protein could be specifically immunoprecipitated with anti-GFP antibody, as seen by 15% SDS−PAGE. (Size of EYFP is 28 kDa while that of the fusion EYFP-Hpx is about 90 kDa. The two figures have been aligned side by side). The upper panel shows the pull-down of [^{35}S] ORF3 protein by *in vivo* expressed EYFP-Hpx. [^{35}S] ORF3 protein was recovered by EYFP-Hpx protein bound to protein A Sepharose beads (lane 3) and not with EYFP alone (lane 1) or when preimmune serum was used (lane 2). Samples were resolved by 15% SDS−PAGE, and ORF3 protein was detected by fluorography. The numbers to the left- and right-hand sides of the panels indicate the position and size of the molecular weight markers in kDa.

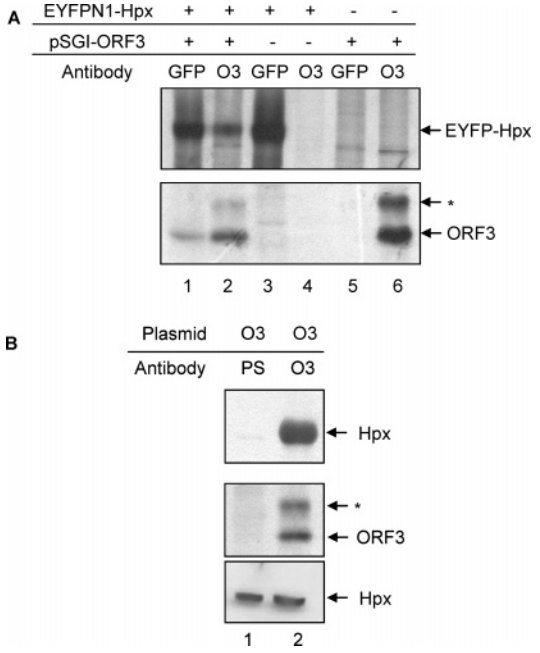

FIGURE 3: EYFP-Hpx protein coprecipitates with ORF3 in mammalian cells. (A) COS-1 cells were cotransfected with EYFPN1-Hpx and pSGI-ORF3 expression constructs (lanes 1 and 2) or with EYFPN1-Hpx (lanes 3 and 4) or with pSGI-ORF3 (lanes 5 and 6) alone. After metabolic labeling the cell lysate was immunoprecipitated with anti-GFP antibody (lanes 1, 3 and 5) or with anti-ORF3 antibody (lanes 2, 4 and 6). Half of the sample was resolved by 8% SDS−PAGE (upper panel), and the other half was resolved by 15% SDS−PAGE (lower panel) followed by fluorography to detect EYFP-Hpx and ORF3 expression, respectively. EYFP-Hpx and ORF3 bands are indicated. EYFP-Hpx and ORF3 co-immunoprecipitate with both GFP and ORF3 antibodies (lanes 1 and 2, respectively). A nonspecific cellular protein, marked by an asterisk, coprecipitates with the ORF3 protein. (B) Endogenous Hpx co-immunoprecipitates with ORF3 in HuH-7 cells. HuH-7 cells were transfected with pSGI-ORF3 expression construct (lanes 1and 2) and metabolically labeled. Half of the total cell lysate was resolved by 8% SDS−PAGE and immunoblotted with anti-hemopexin antibody to detect endogenous Hpx (lower panel), and the other half was immunoprecipitated with polyclonal anti-ORF3 antibody (lane 2) or preimmune serum (lane 1). One half of the immunoprecipitated sample was resolved by 8% SDS−PAGE and immunoblotted with monoclonal anti-hemopexin antibody to detect co-immunoprecipitated hemopexin (upper panel), and the remaining half was resolved by 15% SDS−PAGE followed by fluorography to detect ORF3 expression (middle panel).

with IP buffer, the EYFP-Hpx protein bound to protein A Sepharose beads was mixed with [^{35}S] labeled *in vitro* translated ORF3 protein (expressed from the pSGI-ORF3 construct), incubated for 4 h at 4 °C and the beads were again washed three times in IP buffer. Any ORF3 protein that associated with Hpx was then determined by fluorography. Half of the sample was resolved by 8% (Figure 2B, lower panel) and the other half by 15% SDS−PAGE (Figure 2B, upper panel), to detect EYFP-Hpx expression and recovered ORF3, respectively. EYFP-Hpx fusion protein of expected size, about 90 kDa, was specifically immunoprecipitated with anti-GFP antibody (Figure 2B, lower panel, lane 3) and not with preimmune sera (lane 2). ORF3 was recovered with EYFP-Hpx (upper panel, lane 3). As control, pEYFPN1 plasmid expressing the 28 kDa EYFP protein alone (lower panel, lane 1) was processed simultaneously as above. The results indicated that ORF3 interacts specifically with the Hpx portion of the protein A Sepharose-EYFP-Hpx fusion protein. The binding was reproducible in multiple experiments.

Hpx Co-Immunoprecipitates with ORF3 in Mammalian Cells. The ORF3−Hpx interaction was also confirmed in a mammalian cell environment. In mammalian cells, proteins are more likely to be in their native conformations and to have the appropriate post-translational modifications; therefore results are more likely to represent biologically significant interactions. COS-1 cells were cotransfected with EYFPN1-Hpx and pSGI-ORF3 (Figure 3A, lanes 1 and 2) or EYFPN1-Hpx alone (lanes 3 and 4) or pSGI-ORF3 alone (lanes 5 and 6). After metabolic labeling an equal amount of protein from each sample was immunoprecipitated using anti-ORF3 (lanes 2, 4 and 6) or anti-GFP antibody (lanes 1, 3 and 5). The samples were split into 2 equal halves; one half was resolved by 8% SDS−PAGE (Figure 3A, upper panel) and the other half was resolved by 15% SDS−PAGE

(lower panel) followed by fluorography to detect EYFP-Hpx and ORF3 expression, respectively. EYFP-Hpx co-immunoprecipitated with ORF3 using anti-ORF3 antibody (upper panel, lane 2). Reciprocally using anti-GFP antibody, ORF3 co-immunoprecipitated with EYFP-Hpx (lower panel, lane 1). As negative control, EFPN1-Hpx transfected cell lysate was immunoprecipitated with ORF3 antibody (lane 4) and vice versa, pSGI-ORF3 transfected cell lysate was immunoprecipitated with GFP antibody (lane 5). Lanes 3 and 6 are positive controls for EYFP-Hpx and ORF3 expression, respectively. A nonspecific cellular protein, marked by an asterisk, coprecipitates with the ORF3 protein as has been reported earlier (*19*).

Association of ORF3 with hemopexin was further confirmed in the human hepatoma cell line, HuH-7. These cells were transfected with pSGI-ORF3 expression construct (Figure 3B, lanes 1 and 2). Half of the metabolically labeled total cell lysate was resolved by 8% SDS−PAGE and immunoblotted with anti-hemopexin antibody (mouse monoclonal, Abnova) to detect Hpx expression (lower panel). The results show that the input level of Hpx is the same in the lysates of samples 1 and 2. An equal amount of protein from the rest of each sample was immunoprecipitated using anti-ORF3 antibody (lane 2) or preimmune sera (lane 1). The immunoprecipitated samples were split into two halves; one half was analyzed by 8% SDS−PAGE (upper panel) and immunoblotted with anti-hemopexin antibody to detect co-immunoprecipitated endogenous hemopexin protein, and the other half by 15% SDS−PAGE (middle panel) followed by fluorography to detect ORF3 expression. The ORF3 protein could coprecipitate endogenous hemopexin (upper panel, lane 2). As a negative control, mock transfected cell lysate was immunoprecipitated using anti-ORF3 antibody and immunoblotted with anti-hemopexin antibody to rule out cross-reactivity between Hpx and ORF3-antibody (data not shown). The co-immunoprecipitation studies confirmed that ORF3 associates with endogenous hemopexin.

FRET Measurements of the ORF3−Hpx Interaction. To detect ORF3−Hpx interaction *in vivo* and to complement the results of the *in vitro* interaction assays, we studied the localization of these proteins in transfected COS-1 cells to assess interaction between them microscopically employing FRET. This nonradiative energy transfer follows stringent conditions of distance and dipole orientations between the donor and acceptor fluorophores. The efficiency of energy transfer is inversely proportional to the sixth-power of the distance between donor and acceptor (*24*). Proteins fused to the cyan (ECFP) and yellow (EYFP) colored variants of the EGFP were used as the donor acceptor FRET pair. The ECFPN1-ORF3 and EYFPN1-Hpx constructs were cotransfected into COS-1 cells and imaged for ECFP (green pseudo color) and EYFP (red pseudo color), as shown in Figure 4A, panels I and II, respectively. The distribution of ORF3, as observed earlier (*12*, *13*), was cytoplasmic and displayed punctate staining. The EYFP-Hpx was also cytoplasmic with some perinuclear localization. The ORF3 protein colocalized with Hpx. Effective colocalization resulted in the production of golden yellow color upon superimposition of panel I over II (panel III).

A total of 10 cells were imaged over two separate experiments for FRET analysis. A representative image is shown in Figure 4B. ECFP-ORF3 and EYP-Hpx expression can be seen in panels I and II, respectively. ORF3 protein colocalized with Hpx, as observed by the presence of yellow colored areas in the superimposed image of panel I over panel II (panel III). To make measurements independent of the expression levels of the two fusion proteins, we followed an acceptor photobleach protocol, as described previously (*22*). The mean fluorescence intensity (MFI) from the donor fluorophore (ECFP-ORF3) before and after photobleaching of the acceptor fluorophore (EYFP-Hpx) was recorded, and FRET efficiency was calculated. Panel IV shows ECFP-ORF3 before photobleaching of EYFP-Hpx, and panel V shows the same cell after photobleaching. MFI at two areas within the same cell was recorded, one where the two proteins colocalized (marked A, panels IV and V) and another where no colocalization was observed, i.e., a negative control (marked C). The MFI obtained in the different areas is graphically shown in Figure 4B, before photobleaching (BP) and after photobleaching (AP). An average percent FRET efficiency of 14 ± 4.61 was found in the region of colocalization as opposed to only 1 ± 0.9 in the noncolocalized control area. Since mere colocalization of two proteins is not sufficient to yield energy transfer, the results provide strong *in vivo* support for a physical interaction between the ORF3 and Hpx proteins. In our previous publication (*22*) ECFP-ORF3 and EYFP-ORF3 pair was used as a positive control in the FRET assay. An average percent FRET efficiency of 26.4 ± 7.01 was found in the region of colocalization as opposed to 8.68 ± 4.48 in the noncolocalized control area. Coexpression of ECFP and EYFP vectors alone was used as a negative control for the FRET assay where a low percent FRET efficiency of 1.2 ± 1.19 was observed.

Deletion Mapping of the Interacting Domains of the ORF3 and Hpx Proteins Using the Yeast Two-Hybrid System. To characterize the domains involved in the ORF3−Hpx interaction, an array of deletion mutations were constructed for both ORF3 and Hpx and were cloned into the yeast two-hybrid AD- and BD- vectors. Pairwise combinations of full-length fusion constructs and deletion mutants of each fusion construct were tested for protein−protein interaction by yeast two-hybrid assay. The strength of these interactions was investigated by measuring the relative β-galactosidase activity and by the ability to grow in medium lacking histidine and adenine in the presence of 0, 5, 10 and 20 mM 3-AT. The latter results indicated the strength of the protein−protein interaction as a function of histidine prototrophy. The two truncations of the Hpx protein that express each half separately both showed interaction with full-length ORF3 but with strength 2.6 fold less than the full-length protein. None of the other deletion mutants showed interaction with full-length ORF3 when tested in the yeast two-hybrid system (Figure 5A). On the other hand ORF3 deletion mutants showed both positive and negative results with various different deletion mutants when tested with full-length Hpx for two-hybrid interaction. The ORF3 (1−91) and ORF3 (1−77) truncated proteins gave a positive interaction with full-length Hpx in the yeast two-hybrid assay with strength of interaction comparable to that obtained with full-length ORF3 (1−123). On the other hand, ORF3 (83−123) did not give a positive two-hybrid result. These initial experiments suggested that the region of ORF3 from amino acids 1−77 is involved in the interaction. To further narrow down the

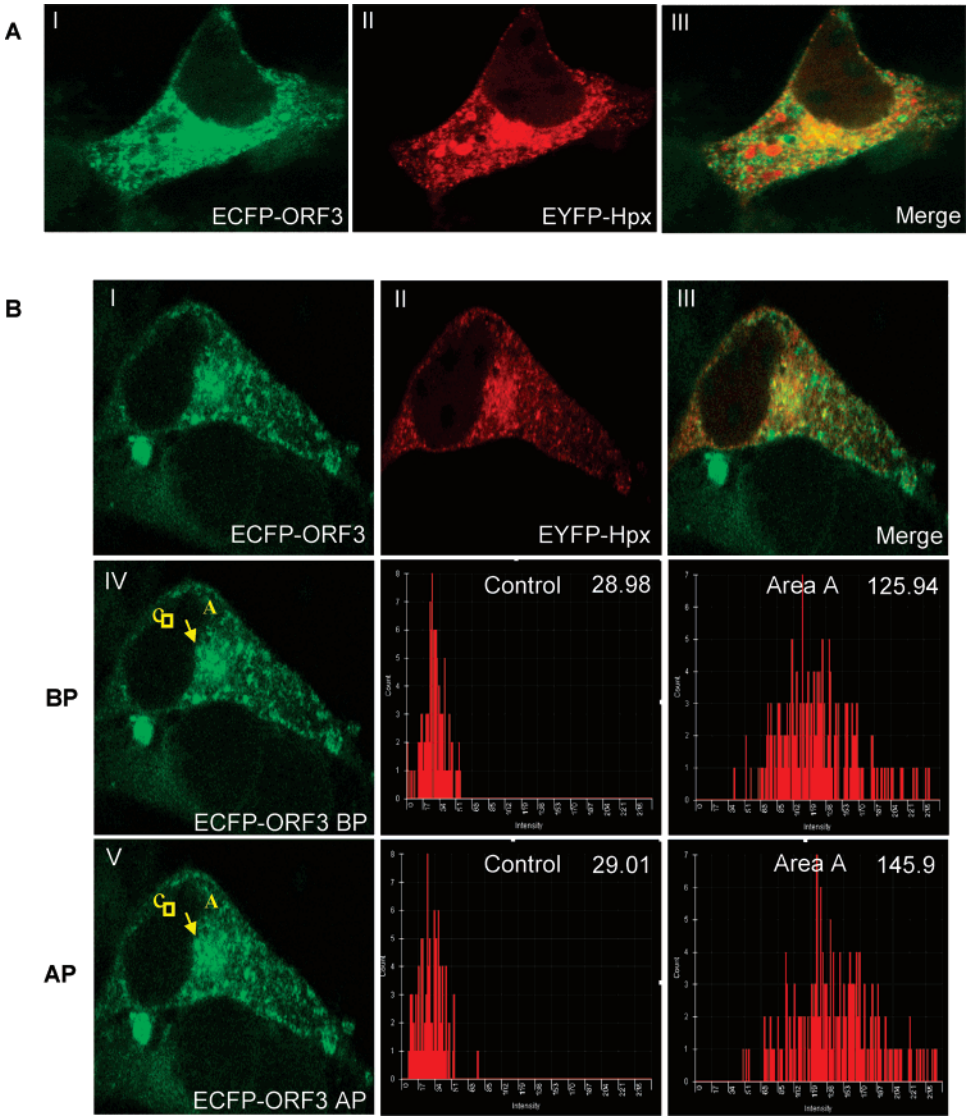

FIGURE 4: Colocalization of ORF3 with Hpx in COS-1 cells and FRET analysis of ORF3−Hpx interaction. (A) COS-1 cells were cotransfected with ECFP-ORF3 and EYFP-Hpx expression constructs. 48 h post-transfection, cells were separately imaged for ECFP (panel I, green pseudocolor) and EYFP (panel II, red pseudocolor). Areas where the two proteins colocalize result in the production of yellow color upon superimposition of panel I over II (panel III). (B) COS-1 cells were cotransfected with ECFP-ORF3 and EYFP-Hpx expression constructs. 48 h post-transfection, cells were separately imaged for ECFP (panel I, green pseudocolor) and EYFP (panel II, red pseudocolor). Areas where the two proteins colocalize result in the production of yellow color upon superimposition of panel I over II (panel III). The ECFP images before photobleach (panel IV) and after EYFP photobleaching (panel V) are shown. Histograms of the mean fluorescence intensity (MFI) of ECFP in the area of colocalization (A) and in the region where the two proteins do not colocalize (C) are shown, either before (BP) or after photobleaching (AP) of EYFP. The numbers on the top right-hand side of these panels indicate the MFI value of that area. Representative images are shown from a total of 10 cells imaged over two separate experiments.

interaction domain, ORF3 (1−63) was studied. Although a positive two-hybrid result was obtained, the strength of interaction was about 2 fold less compared to full-length ORF3 (1−123) as observed from the liquid β-galactosidase assay and ability to grow only up to 10 mM 3-AT. An analysis of these results suggested that amino acids 63 to 77 are involved in the interaction, however, the presence of this region alone is not sufficient to give a positive two-hybrid result. This was evident by the negative two-hybrid results obtained with the deletion construct ORF3 (63−123). ORF3 (33−123) again gave a positive result with strength comparable to full-length ORF3. This implied that the region between amino acids 33 and 63 of ORF3 contains the interaction domain. The results indicated that the minimal region that supported full interaction, as analyzed by yeast two-hybrid assay, was from amino acids 33 to 77. Loss of amino acids 63 to 77 resulted in 50% loss of interaction, but the region 33 to 63 was essential to observe any interaction at all. The interaction domain identified is near ORF3 Ser 80 amino acid residue, which has earlier been shown to be phosphorylated (*11*). To see the effect of phosphorylation on ORF3−Hpx interaction, ORF3 S80A point mutant and the ORF3 protein of the Mexican isolate (both of these proteins are not phosphorylated) were checked for interaction with full-length Hpx. Both the proteins gave a positive two-hybrid assay with Hpx, with strength of interaction comparable to that obtained with full-length ORF3 (1−123) (Figure 5A).

N-Terminal Hydrophobic Domain II of the ORF3 Protein Binds to the Full-Length Hemopexin Protein Assayed by Co-Immunoprecipitation Analysis. The yeast two-hybrid results were verified *in vivo* in COS-1 cells. The ORF3 protein and

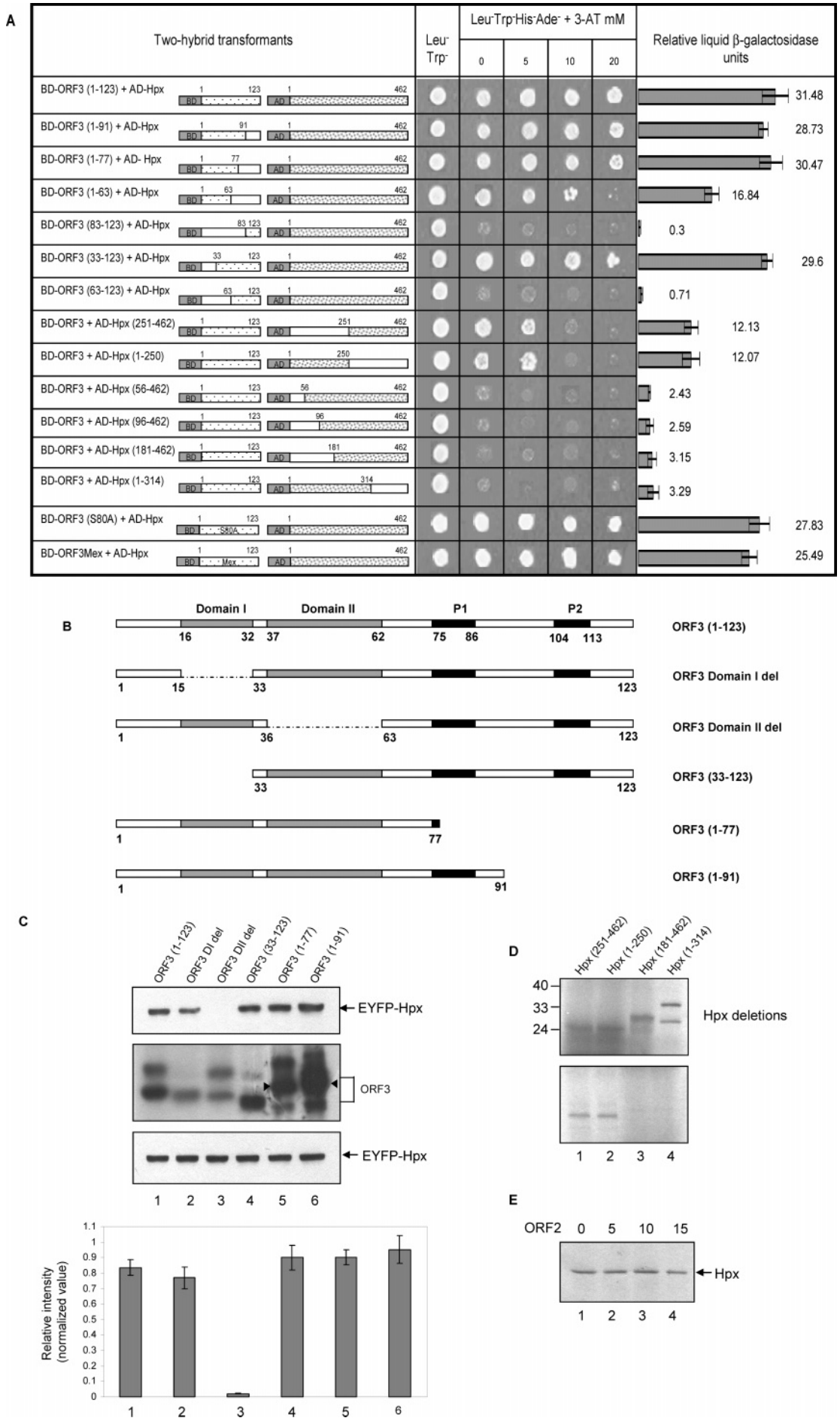
A
Two-hybrid transformants
Leu⁻ Trp⁻
Leu⁻Trp⁻His⁻Ade⁻ + 3-AT mM
0
5
10
20
Relative liquid β-galactosidase units
BD-ORF3 (1-123) + AD-Hpx
31.48
BD-ORF3 (1-91) + AD-Hpx
28.73
BD-ORF3 (1-77) + AD- Hpx
30.47
BD-ORF3 (1-63) + AD-Hpx
16.84
BD-ORF3 (83-123) + AD-Hpx
0.3
BD-ORF3 (33-123) + AD-Hpx
29.6
BD-ORF3 (63-123) + AD-Hpx
0.71
BD-ORF3 + AD-Hpx (251-462)
12.13
BD-ORF3 + AD-Hpx (1-250)
12.07
BD-ORF3 + AD-Hpx (56-462)
2.43
BD-ORF3 + AD-Hpx (96-462)
2.59
BD-ORF3 + AD-Hpx (181-462)
3.15
BD-ORF3 + AD-Hpx (1-314)
3.29
BD-ORF3 (S80A) + AD-Hpx
27.83
BD-ORF3Mex + AD-Hpx
25.49
B
Domain I
Domain II
P1
P2
ORF3 (1-123)
ORF3 Domain I del
ORF3 Domain II del
ORF3 (33-123)
ORF3 (1-77)
ORF3 (1-91)
C
ORF3 (1-123)
ORF3 DI del
ORF3 DII del
ORF3 (33-123)
ORF3 (1-77)
ORF3 (1-91)
EYFP-Hpx
ORF3
EYFP-Hpx
Relative intensity (normalized value)
D
Hpx (251-462)
Hpx (1-250)
Hpx (181-462)
Hpx (1-314)
Hpx deletions
E
ORF2 0 5 10 15
Hpx

its deletion constructs used for expression in mammalian cells have been described under Experimental Procedures and illustrated in Figure 5B. An analysis of the 123 amino acid ORF3 protein shows two N-terminal hydrophobic domains (domains I and II) and the two C-terminal proline-rich regions (P-1 and P-2) (*13*, *25*), which are indicated. These deletions were cotransfected with EYFPN1-Hpx into COS-1 cells. One-third of the metabolically labeled total cell lysate was resolved by 8% SDS−PAGE and immunoblotted with anti-GFP antibody to detect EYFP-Hpx expression (Figure 5C, lower panel), and the rest of the sample was immunoprecipitated using either ORF3 antibody [for ORF3 (1−123), ORF3 DI del, ORF3 DII del and ORF3 (33−123)] or anti-his tag antibody [for ORF3 (1−77) and ORF3 (1−91)]. The C-terminal ORF3 deletions (1−77) and (1−91) express truncated proteins with an N-terminal fusion of a hexa histidine tag as well as a phage T7 gene 10 epitope (*11*). This design was used to enable the immunoprecipitation of C-terminally deleted versions of ORF3, since the anti-ORF3 rabbit polyclonal antibody used in the study predominantly recognizes the immunodominant region encompassing residues 90−123 (*11*). One half of the immunoprecipitated sample was resolved by 8% SDS−PAGE and immunoblotted with anti-GFP antibody to detect co-immunoprecipitated EYFP-Hpx (Figure 5C, upper panel) and the remaining half was resolved by 15% SDS−PAGE followed by fluorography to detect ORF3 expression (Figure 5C, middle panel). As expected, the ORF3 full-length protein was able to associate with and hence pull-down Hpx (Figure 5C, upper panel, lane 1). The ORF3 truncated proteins including amino acids 33−123, 1−77 and 1−91 and the Domain I deleted construct could also pull-down Hpx (Figure 5C, upper panel, lanes 4, 5, 6 and 2, respectively). These results corroborated with the yeast two-hybrid results. Further the ORF3 mutant, in which domain II has been specifically deleted, did not co-immunoprecipitate Hpx (upper panel, lane 3). The middle panel shows the expression of the ORF3 protein and its deletions in corresponding samples. The equal intensities of the EYFP-Hpx band in all the lanes in the lower panel show that the Hpx fusion protein expression is equal in all the transfected samples. Together, these experiments confirm that the hydrophobic domain II of the ORF3 protein, spanning amino acids 37 to 62, is responsible for interacting with Hpx. There were quantitative differences between the amount of ORF3 protein and its deletions expressed in cells (compare lanes 1−6, middle panel) and hence also in the amount of EYFP-Hpx associated with them (compare lanes 1−6, upper panel). The different expression levels of the ORF3 truncations could also be the result of possibly different specificities of the antibodies used to immunoprecipitate the truncated proteins. Densitometry analysis was thus conducted to quantify the amount of protein that was pulled-down. Densitometry analyses were made using ImageJ software V. 1.36b supported by Wayne Rasband (National Institutes of Health,) by integrating intensities of all the pixels in the band excluding the background. To normalize for different expression levels, the data is reported graphically as the ratio of the band intensity of the Hpx protein co-immunoprecipitated in the individual lanes in the upper panel to the band intensity of the ORF3 protein (full length or its truncations) in the corresponding lanes in the middle panel (Figure 5C). The domain II deleted mutant reproducibly showed no co-immunoprecipitation of Hpx protein.

In the yeast two-hybrid assay, only the N- and C-terminal Hpx truncations showed interaction with full-length ORF3 (Figure 5A). Due to differences in the yeast cell physiology and *in vitro* interaction assays, Hpx protein truncations were checked for interaction with ORF3 by the *in vitro* histidine pull-down assay also, as described under Experimental Procedures. Expression of Hpx truncations (251−462), (1−250), (181−462) and (1−314) from the pSGI expression constructs was verified using *in vitro* coupled transcription−translation to produce [^{35}S] labeled protein of the expected molecular weights as detected by fluorography (Figure 5D,

FIGURE 5: Deletion mapping of the regions in ORF3 and Hpx responsible for interaction. (A) Mapping using the yeast two-hybrid system. The deletion mutants constructed for ORF3 and Hpx were cloned into pAS2 (BD-) or pACT2 (AD-) yeast two-hybrid vectors, respectively, and tested for their ability to interact with full-length AD-Hpx or BD-ORF3. The first column gives the overview of the deletion mutants that were assayed. The numbers above the boxes represent the first and the last amino acid of the regions included in the truncated protein. BD-ORF3 (S80A) is the ORF3 Ser80Ala point mutant and BD-ORF3Mex is the protein from the Mexican isolate. All abbreviations used are as described in Figure 1. Interaction data obtained with co-transformants that are able to grow in leu$^-$trp$^-$ medium is shown. Interactions were assayed for histidine and adenine prototrophy (ability to grow in leu$^-$trp$^-$his$^-$ade$^-$ medium) in the presence of 0, 5, 10 or 20 mM 3-AT. The horizontal bar graph represents relative β-galactosidase units determined from the liquid β-gal assay. (B) The ORF3 protein and its mutants assayed for interaction with EYFP-Hpx *in vivo* by co-immunoprecipiattion analysis are illustrated. The two N-terminal hydrophobic domains, domains I and II, and the two C-terminal proline-rich regions (P1 and P2) are shown for the full-length protein. The numbers indicate the amino acids at the boundaries of the various domains, regions and mutants. (C) Co-immunoprecipitation assay showing ORF3−Hpx interaction. The full-length ORF3 and its various deletions described above were cotransfected with EYFPN1-Hpx into COS-1 cells. 44 h post-transfection, cells were labeled with [^{35}S] cys/met labeling mix for 4 h and then harvested in IP buffer. One-third of the total cell lysate was resolved by 8% SDS−PAGE and immunoblotted with anti-GFP antibody to detect EYFP-Hpx expression (lower panel). The lower panel shows the Hpx fusion protein expression is equal in all the transfected samples. The rest of the sample was immunoprecipitated using anti-ORF3 antibody (lanes 1, 2, 3 and 4) or anti-his tag antibody (lanes 5 and 6). One half of the immunoprecipitated sample was resolved by 8% SDS−PAGE and immunoblotted with anti-GFP antibody to detect co-immunoprecipitated EYFP-Hpx (upper panel), and the remaining half was resolved by 15% SDS−PAGE followed by fluorography to detect ORF3 expression (middle panel). The ORF3 (1−77) and ORF3 (1−91) bands are indicated with an arrowhead (lanes 5 and 6, respectively, middle panel). ORF3 full-length (1−123), domain I deleted (ORF3 DI del), ORF3 domain II deleted (ORF3 DII del), ORF3 (33−123) and ORF3 (1−77) expressed proteins are the lower bands clearly seen in lanes 1, 2, 3 and 4, respectively. EYFP-Hpx band is indicated. The interaction data is reported graphically as the ratio of Hpx band intensity (upper panel) in each lane to that of the corresponding expressed ORF3 full-length protein or its truncation (middle panel). (D) The upper panel is a control gel showing Hpx deletions expressed using coupled transcription−translation system. Major bands show the expressed proteins of interest and correspond to their calculated molecular weight. The numbers to the left-hand side of the panel indicate the position and size of the molecular weight markers in kDa. The lower panel shows Hpx (251−462) and (1−250) interact with ORF3 (lanes 1 and 2, respectively) in *in vitro* histidine pull-down assay. (E) *In vitro* histidine pull-down assay to study ORF3−Hpx interaction as described in Figure 2, but in the presence of increasing amount of *in vitro* expressed cold ORF2 protein. Lane 1 shows the Hpx protein recovered by His_6-ORF3 in absence of exogenously added ORF2. Lanes 2, 3 and 4 show the Hpx binding when 5, 10 and 15 μL ORF2, respectively, is added.

upper panel). The labeled Hpx proteins were then incubated with Ni-NTA beads to which His_6-ORF3 was bound. Results obtained corroborated our yeast two-hybrid data. Only the two N- and C-terminal truncations of the Hpx protein were recovered by the Ni-NTA-His_6-ORF3 fusion protein (Figure 5D, lower panel, lanes 1 and 2), while the truncations larger than these do not support interaction (lanes 3 and 4).

The interaction domain found in our studies, involving domain II and amino acids 63−77, partially overlaps with the region in the ORF3 protein (amino acids 57−81) known to interact with ORF2 (*12*). This prompted us to ask whether the ORF3−ORF2 interaction had any bearing on the ORF3−Hpx interaction. For this a competition assay was done where, in the *in vitro* histidine pull-down assay, increasing amounts of *in vitro* transcribed−translated cold ORF2 were added and the effect of the addition of ORF2 on ORF3−Hpx interaction was observed. The results are shown in Figure 5E. It was observed that addition of 5 or 10 μL of ORF2 TNT reaction did not inhibit Hpx binding to ORF3 (compare lanes 2 and 3 with lane 1). However addition of 15 μL ORF2 (lane 4) to the pull-down reaction slightly decreased the amount of Hpx protein recovered by His_6-ORF3.

DISCUSSION

HEV *per se* is a poorly studied virus. Subgenomic expression strategies have been used to study the properties and functions of individual HEV gene products toward understanding their role in viral replication and pathogenesis (*9*, *11*, *19*). For our study also, as has been done for all previous published reports, we expressed the ORF3 protein in cells and studied its interaction with hemopexin. There have been no reports so far that have studied the physiological levels of ORF3 either in patient samples or in animal models. Previous studies suggest that ORF3 has multifarious activities that involve its interactions with host cellular proteins (*11*, *13*, *22*). In the present study we identified Hpx as a novel interacting partner of ORF3 protein of HEV by using a yeast two-hybrid screen. We verified Hpx to be a true positive by performing retests independently with pAS2-ORF3 (BD-ORF3) bait or an empty pAS2 (BD-) plasmid. Truly positive AD/library plasmids activate reporter genes only when the original bait plasmid is also present. Yeast mating experiments and domain swapping further demonstrated specificity of the interactions.

In vitro pull-down assays were employed to validate ORF3−Hpx interaction. Reciprocal co-immunoprecipitation assays also clearly indicated the direct interaction between the two proteins in transfected COS-1 cells. It was also demonstrated that ORF3 interacts with endogenous Hpx in human hepatoma cells. Further in COS-1 cells the Hpx and ORF3 proteins were shown to colocalize. It is important to note here that although most of the ORF3 and Hpx proteins imaged colocalize (as can be seen by the presence of yellow spots in the merged panels in Figure 4), there are regions in the cell where no colocalization was observed. This is expected as Hpx, a secreted protein, would have the classical ER/Golgi/vesicles distribution. For ORF3 the exact cellular localization is not well established. So it is likely that the two proteins are in the same cellular compartment at some stage of the trafficking event or normal cellular processing of these proteins, where colocalization occurs. On the other hand mere colocalization of two proteins does not imply that they interact. Interaction between these proteins was thus confirmed by *in vivo* FRET measurements (*26*) using ECFP (donor) and EYFP (acceptor) fused upstream to ORF3 and Hpx, respectively. The ECFP−EYFP pair is a commonly used donor−acceptor pair ideally suited for FRET measurements. FRET exploits the ability of the higher energy donor fluorophore (ECFP) to transfer some of its energy to the acceptor fluorophore (EYFP) in its excited state. Following FRET, there is a reduction in the donor emission due to the transfer of energy and an increase in the acceptor emission. However, in the acceptor photobleaching method used in this study, after photobleaching of the EYFP acceptor, there should be an increase in emission from the ECFP donor if FRET is taking place. This is because the acceptor fluorophore is no longer able to quench the donor emission. Based on this method, we show here significant percent FRET efficiency of 14 ± 4.61 between ECFP-ORF3 and EYFP-Hpx, supporting the *in vitro* results that ORF3 and Hpx interact with each other.

The critical regions for protein−protein interaction were mapped by yeast two-hybrid and *in vivo* co-immunoprecipitation assays carried out in the presence of different deletion mutants of ORF3 and Hpx. Specifically, the N-terminal hydrophobic region of the ORF3 molecule, comprising amino acid residues 37 to 62, was identified as the domain responsible for interaction, since the protein lacking this region failed to interact with full-length Hpx in both the yeast two-hybrid and co-immunoprecipitation assay. This region of ORF3, domain II, is the second of its two N-terminal hydrophobic domains and is rich in aliphatic and aromatic hydrophobic residues. Our yeast two-hybrid data also suggested that amino acids 63 to 77 possibly contribute to the strength of the interaction. In the yeast two-hybrid assay C-terminally truncated ORF3 protein, ORF3 (1−77) and ORF3 (1−91), as well as the N-terminally truncated ORF3 (33−123), were convincingly demonstrated to interact with full-length Hpx as strongly as does the full-length ORF3 protein. Also, both the phosphorylation deficient constructs of ORF3 [ORF3 (S80A) and ORF3Mex] interacted with Hpx, indicating that phosphorylation of ORF3 is not a prerequisite for ORF3−Hpx interaction. In co-immunoprecipitation assays from transfected COS-1 cells also the full-length ORF3 and its mutants (except domain II deletion) were shown to interact with Hpx. Further, unlike the equal expression of YFP-Hpx in all transfected samples, the different ORF3 deletion constructs expressed unequal protein amounts. ORF3 (33−123), ORF3 (1−77) and ORF3 (1−91) constructs expressed higher levels of protein followed by the full-length expression construct, and comparatively lesser protein expression was obtained for DI and DII deletions. This could be a consequence of the two different antibodies used and also the specificity of each toward the different truncations. Interestingly the interaction domain found in our studies, involving domain II and amino acids 63−77, partially overlaps with the region in the ORF3 protein (amino acids 57−81) known to interact with ORF2 (*12*). Strategic overlapping of the interaction domains may be a possible mechanism to ensure regulation of these interactions. Steric hindrance may ensure only one interaction at a given time. Alternatively, these interactions might be far removed from

each other in the cell, spatially or temporally, and hence each may bear no relation to the other whatsoever. In the *in vitro* pull-down assay it was observed that only a very high input of ORF2 protein could slightly inhibit the ORF3−Hpx binding. This suggests that the ORF3−ORF2 and ORF3−Hpx interaction may be mutually exclusive or spatially or temporally removed from each other in the cell. Further the ORF3−ORF2 interaction requires ORF3 to be phosphorylated (*12*) which is not a prerequisite for ORF3−Hpx interaction as shown by the yeast two-hybrid assay. Also our data suggests that ORF3 can interact with Hpx irrespective of its glycosylation status. Endogenous Hpx and that expressed in transfected COS-1 cells is glycosylated while the TNT expressed protein is not. However, ORF3 has been shown to preferentially interact with the non-glycosylated form of ORF2 (*12*). Thus in our study the known ORF3−ORF2 interaction has been shown not to have any effect on ORF3−Hpx interaction.

According to UniProt (the universal protein knowledge base, http://www.ebi.uniprot.org) the human Hpx protein (primary accession number P02790) contains 5 hemopexin-like domains/hemopexin-type repeats, spanning amino acids 56−95, 97−141, 188−231, 263−306 and 308−353. Several deletion constructs of Hpx were made designed around these regions, and tested for their ability to interact with the full-length ORF3. Attempts to identify interacting domains in the Hpx polypeptide failed, and none of the deletions tested retained the ability of the protein to associate with ORF3 in the yeast two-hybrid assay or in *in vitro* pull-down assay. Perhaps the smaller truncations occur within the same subunit and are therefore highly dependent on the 3-D structure of the whole protein in order to bring different parts of the peptide into close proximity, thus disrupting the conformation and also abolishing the interaction. Only the two large truncations of Hpx, which divide the molecule into the two structurally similar halves, the N- and C-terminal Hpx domains (*18*, *27*, *28*), showed positive in yeast two-hybrid assay, but with strengths nearly 3 fold less than full-length. These two truncations also interacted with ORF3 in *in vitro* assay.

The Hpx protein, mainly produced by the parenchymal cells of the liver, consists of a single polypeptide chain containing 439 amino acids residues (excluding the 23 amino acid signal sequence), with six intrachain disulfide bridges (*18*, *27*, *28*). It is heavily glycosylated protein with 20% carbohydrates. Hpx is an acute phase protein and is the major heme transporter in plasma, is a player in iron homeostasis and also regulates gene expression (*29*) to promote cell survival. These activities of Hpx become significant during acute infection (*30*). Hence the interaction of ORF3 with Hpx may interfere with the latter's role as an acute phase reactant.

Heme in circulation is rapidly sequestered by Hpx and in doing so Hpx protects cells against hemoglobin-mediated oxidative damage during intravascular hemolysis. A case of acute viral hepatitis E has been reported with severe intravascular hemolysis (*31*). Under such conditions, the ORF3−Hpx interaction may be significant to viral pathogenesis, as evidenced by a defective recovery and severe renal damage after acute hemolysis in Hpx deficient mice (*32*). Hpx protects cells against heme-mediated damage by activating N-terminal c-jun kinase and the antiapoptotic transcription factor NFκB (*33*). Further, Hpx plays an important link between heme and iron metabolism and together with haptoglobin and transferrin maintains iron homeostasis (*34*). ORF3−Hpx interaction may disturb this balance toward viral benefit as seen with some other viruses. There are reports that show that iron deposition in hepatocytes facilitates viral infection (*35*) and that viral infection increases serum ferritin concentration and increases iron accumulation in several tissues (*36*). In *in vitro* experiments also, levels of iron have been reported to influence viral replication (*37*).

In our studies, the interesting and possibly significant observation was the weak interaction that was obtained between ORF3 and the two Hpx domains. Analysis of the internal homology in amino acid sequence indicates that Hpx comprises two homologous domains (with about 25% amino acid identity) of about 200 residues each (spanning amino acid regions 48 to 238 and 256 to 462), joined by a 20 residue linker. Each of the two Hpx domains is in turn made up of several Hpx-type repeats of about 35−45 residues (*38*). Hpx domains are also found as C-terminal domains in matrix metalloproteinases (MMPs) and are a common structural motif found in all but two MMPs (MMP-7 and MMP-26). MMPs are Zn^{2+}- and Ca^{2+}-dependent endopeptidases, which function in the turnover of ECM components. MMPs also have diverse roles in modulating the immune response to infection. They facilitate leukocyte recruitment, cytokine and chemokine processing and defensin activation (*39*). Despite the overall structural similarity of all Hpx-like domains, they possess many different properties that are MMP specific. For instance the Hpx domain has been shown to function in protein substrate recognition (*40*) and in enzymatic regulation and subcellular localization of MTI-MMP (*41*, *42*) while the Hpx-like domain of MMP-9 is an antagonist of enzyme activity (*43*).

Two Hpx-like domains are also present in vitronectin, a matrix glycoprotein. Liang et al. identified by phage display a hydrophobic pentapeptide motif within the Hpx-type repeats of vitronectin to be recognized by specific surface components of *Streptococcus pyogenes* cells (*44*). Moreover cells of *S. pyogenes* were shown to bind to the synthetic peptide as well as to immobilized Hpx, which have structural homology to the Hpx-type repeats in the vitronectin molecule. Further, solubilized vitronectin inhibited binding to Hpx. Thus *S. pyogenes* cells can bind to Hpx-like domains of both vitronectin and Hpx since they are structurally homologous. Likewise, since ORF3 was shown unequivocally to bind Hpx and its two domains, other Hpx-domain containing proteins, like MMPs, could also be potential targets for ORF3 binding. By binding to MMPs Hpx-like domains, ORF3 could modulate many of the activities of MMPs that have been shown to have an important role in the normal immune response to infection (*39*, *45*, *46*).

In our previous publications (*14*−*16*), we have shown that ORF3 interacts with α_1-microglobulin and bikunin and possibly creates an immunosuppressive environment around the infected liver cell. In the present study, we identified yet another host protein, hemopexin, which interacts with ORF3. Hpx plays important roles in inflammation, and the Hpx-like domain containing MMPs modulate immune response to infection. Further, the importance of Hpx domains in these different proteins, with different functions attributed

to the Hpx domain in each, cannot be understated. Hence the ORF3−Hpx interaction must have significant bearing on viral pathogenesis. A future study of viral pathogenesis will reveal the physiological significance of this interaction *in vivo*.

ACKNOWLEDGMENT

Technical help from Ravinder Kumar, Md. Zafrullah and Vaibhao Janbandhu is greatly acknowledged. R.R. was a senior research fellow of the Council of Scientific and Industrial Research, India. A.K.-R. was a postdoctoral fellow supported by the Welcome Trust.

REFERENCES

1. Khuroo, M. S., Teli, M. R., Skidmore, S., Sofi, M. A., and Khuroo, M. I. (1981) Incidence and severity of viral hepatitis in pregnancy, *Am. J. Med. 70*, 252−255.
2. Purcell, R. H., and Emerson, S. U. (2000) Hepatitis E virus infection, *Lancet 355*, 578.
3. Purcell, R. H., and Emerson, S. U. (2001) Hepatitis E Virus, in *Fields Virology* (Knipe, D. M., Howley, P. M., Griffin, D. E., Lamb, R. A., Martin, M. A., Roizman, B., and Straus, S. E., Eds.) 4th ed., pp 3051−3061, Lippincott/The Williams & Wilkins Co. Philadelphia, PA.
4. Schlauder, G. G., Dawson, G. J., Erker, J. C., Kwo, P. Y., Knigge, M. F., Smalley, D. L., Rosenblatt, J. E., Desai, S. M., and Mushahwar, I. K. (1998) The sequence and phylogenetic analysis of a novel hepatitis E virus isolated from a patient with acute hepatitis reported in the United States, *J. Gen. Virol. 79* (Part 3), 447−456.
5. Schlauder, G. G., Desai, S. M., Zanetti, A. R., Tassopoulos, N. C., and Mushahwar, I. K. (1999) Novel hepatitis E virus (HEV) isolates from Europe: evidence for additional genotypes of HEV, *J. Med. Virol. 57*, 243−251.
6. Mansuy, J. M., Peron, J. M., Abravanel, F., Poirson, H., Dubois, M., Miedouge, M., Vischi, F., Alric, L., Vinel, J. P., and Izopet, J. (2004) Hepatitis E in the south west of France in individuals who have never visited an endemic area, *J. Med. Virol. 74*, 419−424.
7. Tei, S., Kitajima, N., Takahashi, K., and Mishiro, S. (2003) Zoonotic transmission of hepatitis E virus from deer to human beings, *Lancet 362*, 371−373.
8. Koonin, E. V., Gorbalenya, A. E., Purdy, M. A., Rozanov, M. N., Reyes, G. R., and Bradley, D. W. (1992) Computer-assisted assignment of functional domains in the nonstructural polyprotein of hepatitis E virus: delineation of an additional group of positive-strand RNA plant and animal viruses, *Proc. Natl. Acad. Sci. U.S.A. 89*, 8259−8263.
9. Zafrullah, M., Ozdener, M. H., Kumar, R., Panda, S. K., and Jameel, S. (1999) Mutational analysis of glycosylation, membrane translocation, and cell surface expression of the hepatitis E virus ORF2 protein, *J. Virol. 73*, 4074−4082.
10. Surjit, M., Jameel, S., and Lal, S. K. (2004) The ORF2 protein of hepatitis E virus binds the 5′ region of viral RNA, *J. Virol. 78*, 320−328.
11. Zafrullah, M., Ozdener, M. H., Panda, S. K., and Jameel, S. (1997) The ORF3 protein of hepatitis E virus is a phosphoprotein that associates with the cytoskeleton, *J. Virol. 71*, 9045−9053.
12. Tyagi, S., Korkaya, H., Zafrullah, M., Jameel, S., and Lal, S. K. (2002) The phosphorylated form of the ORF3 protein of hepatitis E virus interacts with its non-glycosylated form of the major capsid protein, ORF2, *J. Biol. Chem. 277*, 22759−22767.
13. Korkaya, H., Jameel, S., Gupta, D., Tyagi, S., Kumar, R., Zafrullah, M., Mazumdar, M., Lal, S. K., Xiaofang, L., Sehgal, D., Das, S. R., and Sahal, D. (2001) The ORF3 protein of hepatitis E virus binds to Src homology 3 domains and activates MAPK, *J. Biol. Chem. 276*, 42389−42400.
14. Tyagi, S., Surjit, M., Roy, A. K., Jameel, S., and Lal, S. K. (2004) The ORF3 protein of hepatitis E virus interacts with liver-specific alpha1-microglobulin and its precursor alpha1-microglobulin/bikunin precursor (AMBP) and expedites their export from the hepatocyte, *J. Biol. Chem. 279*, 29308−29319.
15. Tyagi, S., Surjit, M., and Lal, S. K. (2005) The 41-amino-acid C-terminal region of the hepatitis E virus ORF3 protein interacts with bikunin, a kunitz-type serine protease inhibitor, *J. Virol. 79*, 12081−12087.
16. Surjit, M., Oberoi, R., Kumar, R., and Lal, S. K. (2006) Enhanced alpha1 microglobulin secretion from Hepatitis E virus ORF3-expressing human hepatoma cells is mediated by the tumor susceptibility gene 101, *J. Biol. Chem. 281*, 8135−8142.
17. Chien, C. T., Bartel, P. L., Sternglanz, R., and Fields, S. (1991) The two-hybrid system: a method to identify and clone genes for proteins that interact with a protein of interest, *Proc. Natl. Acad. Sci. U.S.A. 88*, 9578−9582.
18. Tolosano, E., and Altruda, F. (2002) Hemopexin: structure, function, and regulation, *DNA Cell Biol. 21*, 297−306.
19. Jameel, S., Zafrullah, M., Ozdener, M. H., and Panda, S. K. (1996) Expression in animal cells and characterization of the hepatitis E virus structural proteins, *J. Virol. 70*, 207−216.
20. Panda, S. K., Nanda, S. K., Zafrullah, M., Ansari, I. H., Ozdener, M. H., and Jameel, S. (1995) An Indian strain of hepatitis E virus (HEV): cloning, sequence, and expression of structural region and antibody responses in sera from individuals from an area of high-level HEV endemicity, *J. Clin. Microbiol. 33*, 2653−2659.
21. Sambrook, J., Fritsch, E. F., and Maniatis, T. (1989) *Molecular Cloning: A laboratory manual*, 2nd ed., Cold Spring Harbor Laboratory, Cold Spring Harbor, NY.
22. Kar-Roy, A., Korkaya, H., Oberoi, R., Lal, S. K., and Jameel, S. (2004) The hepatitis E virus open reading frame 3 protein activates ERK through binding and inhibition of the MAPK phosphatase, *J. Biol. Chem. 279*, 28345−28357.
23. Tyagi, S., Jameel, S., and Lal, S. K. (2001) Self-association and mapping of the interaction domain of hepatitis E virus ORF3 protein, *J. Virol. 75*, 2493−2498.
24. Siegel, R. M., Chan, F. K., Zacharias, D. A., Swofford, R., Holmes, K. L., Tsien, R. Y., and Lenardo, M. J. (2000) Measurement of molecular interactions in living cells by fluorescence resonance energy transfer between variants of the green fluorescent protein, *Sci. STKE* **2000**, PL1.
25. Zafrullah, M., Korkaya, H., Xiaofang, L., Kumar, R., and Jameel, S. (2000) Functional Characterization of Hepatitis E Virus Structural Proteins, in *Advances in Animal Virology* (Jameel, S., and Villarreal, L. Eds.), pp 67−83, Oxford & IBH Publishing Co. Pvt. Ltd., New Delhi, India.
26. Truong, K., and Ikura, M. (2001) The use of FRET imaging microscopy to detect protein-protein interactions and protein conformational changes in vivo, *Curr. Opin. Struct. Biol. 11*, 573−578.
27. Altruda, F., Poli, V., Restagno, G., Argos, P., Cortese, R., and Silengo, L. (1985) The primary structure of human hemopexin deduced from cDNA sequence: evidence for internal, repeating homology, *Nucleic Acids Res. 13*, 3841−3859.
28. Altruda, F., Poli, V., Restagno, G., and Silengo, L. (1988) Structure of the human hemopexin gene and evidence for intron-mediated evolution, *J. Mol. Evol. 27*, 102−108.
29. Alam, J., and Smith, A. (1992) Heme-hemopexin-mediated induction of metallothionein gene expression, *J. Biol. Chem. 267*, 16379−16384.
30. Delanghe, J. R., and Langlois, M. R. (2001) Hemopexin: a review of biological aspects and the role in laboratory medicine, *Clin. Chim. Acta 312*, 13−23.
31. Singhvi, D., Gulati, S., Gupta, S., Govil, A., and Purohit, R. (2001) Hemolysis causing marked bilirubinemia in a case of acute viral hepatitis (AVH) with glucose-6 phosphate dehydrogenase deficiency, *Antiseptic 98*, 139−140.
32. Tolosano, E., Hirsch, E., Patrucco, E., Camaschella, C., Navone, R., Silengo, L., and Altruda, F. (1999) Defective recovery and severe renal damage after acute hemolysis in hemopexin-deficient mice, *Blood 94*, 3906−3914.
33. Eskew, J. D., Vanacore, R. M., Sung, L., Morales, P. J., and Smith, A. (1999) Cellular protection mechanisms against extracellular heme. heme-hemopexin, but not free heme, activates the N-terminal c-jun kinase, *J. Biol. Chem. 274*, 638−648.
34. Hentze, M. W., and Kuhn, L. C. (1996) Molecular control of vertebrate iron metabolism: mRNA-based regulatory circuits operated by iron, nitric oxide, and oxidative stress, *Proc. Natl. Acad. Sci. U.S.A. 93*, 8175−8182.
35. Martinelli, A. L., Filho, A. B., Franco, R. F., Tavella, M. H., Ramalho, L. N., Zucoloto, S., Rodrigues, S. S., and Zago, M. A. (2004) Liver iron deposits in hepatitis B patients: association with severity of liver disease but not with hemochromatosis gene mutations, *J. Gastroenterol. Hepatol. 19*, 1036−1041.

36. Distante, S., Bjoro, K., Hellum, K. B., Myrvang, B., Berg, J. P., Skaug, K., Raknerud, N., and Bell, H. (2002) Raised serum ferritin predicts non-response to interferon and ribavirin treatment in patients with chronic hepatitis C infection, *Liver 22*, 269−275.
37. Kakizaki, S., Takagi, H., Horiguchi, N., Toyoda, M., Takayama, H., Nagamine, T., Mori, M., and Kato, N. (2000) Iron enhances hepatitis C virus replication in cultured human hepatocytes, *Liver 20*, 125−128.
38. Jenne, D., and Stanley, K. K. (1987) Nucleotide sequence and organization of the human S-protein gene: repeating peptide motifs in the "pexin" family and a model for their evolution, *Biochemistry 26*, 6735−6742.
39. Parks, W. C., Wilson, C. L., and Lopez-Boado, Y. S. (2004) Matrix metalloproteinases as modulators of inflammation and innate immunity, *Nat. Rev. Immunol. 4*, 617−629.
40. Murphy, G., and Knauper, V. (1997) Relating matrix metalloproteinase structure to function: why the "hemopexin" domain, *Matrix Biol. 15*, 511−518.
41. Lehti, K., Lohi, J., Juntunen, M. M., Pei, D., and Keski-Oja, J. (2002) Oligomerization through hemopexin and cytoplasmic domains regulates the activity and turnover of membrane-type 1 matrix metalloproteinase, *J. Biol. Chem. 277*, 8440−8448.
42. Mori, H., Tomari, T., Koshikawa, N., Kajita, M., Itoh, Y., Sato, H., Tojo, H., Yana, I., and Seiki, M. (2002) CD44 directs membrane-type 1 matrix metalloproteinase to lamellipodia by associating with its hemopexin-like domain, *EMBO J. 21*, 3949−3959.
43. Roeb, E., Schleinkofer, K., Kernebeck, T., Potsch, S., Jansen, B., Behrmann, I., Matern, S., and Grotzinger, J. (2002) The matrix metalloproteinase 9 (mmp-9) hemopexin domain is a novel gelatin binding domain and acts as an antagonist, *J. Biol. Chem. 277*, 50326−50332.
44. Liang, O. D., Preissner, K. T., and Chhatwal, G. S. (1997) The hemopexin-type repeats of human vitronectin are recognized by Streptococcus pyogenes, *Biochem. Biophys. Res. Commun. 234*, 445−449.
45. Das, S., Mandal, M., Chakraborti, T., Mandal, A., and Chakraborti, S. (2003) Structure and evolutionary aspects of matrix metalloproteinases: a brief overview, *Mol. Cell. Biochem. 253*, 31−40.
46. McCawley, L. J., and Matrisian, L. M. (2001) Matrix metalloproteinases: they're not just for matrix anymore!, *Curr. Opin. Cell Biol. 13*, 534−540.

BI7016552